2023 IEEE International Conference on Robotics and Automation (ICRA 2023)
May 29 - June 2, 2023. London, UK

Vitreoretinal Surgical Robotic System with Autonomous Orbital Manipulation using Vector-Field Inequalities

Yuki Koyama, Murilo M. Marinho, and Kanako Harada

***Abstract*— Vitreoretinal surgery pertains to the treatment of delicate tissues on the fundus of the eye using thin instruments. Surgeons frequently rotate the eye during surgery, which is called orbital manipulation, to observe regions around the fundus without moving the patient. In this paper, we propose the autonomous orbital manipulation of the eye in robot-assisted vitreoretinal surgery with our tele-operated surgical system. In a simulation study, we preliminarily investigated the increase in the manipulability of our system using orbital manipulation. Furthermore, we demonstrated the feasibility of our method in experiments with a physical robot and a realistic eye model, showing an increase in the view-able area of the fundus when compared to a conventional technique. Source code and minimal example available at `https://github.com/mmmarinho/icra2023_orbitalmanipulation`.**

I. Introduction

Vitreoretinal surgery is among the most challenging microsurgeries. Tasks require a high level of manipulation skill with two surgical instruments; a dominant instrument, such as a 0.5 mm (25 gauge) diameter forceps or needle, and a light guide to illuminate the workspace. With these instruments, surgeons need to peel off 2.5 μm thick inner-limiting membranes or insert a needle into 100 μm diameter retinal blood vessels. Moreover, hand tremors with an average amplitude of approximately 100 μm [1] make these procedures more difficult.

To address these difficulties, several robotic systems have been developed [2]. These systems can be classified into three fundamentally different approaches: hand-held robotic devices [3], [4], cooperatively-controlled systems [5], [6], and tele-operated systems [7]–[9]. Furthermore, some systems were already used in clinical settings [10], [11].

Most robotic systems generate, either through hardware or software constraints, a fixed *remote center-of-motion* (RCM). RCMs are required for the instruments to move through incisions and prevent damage to the patient. In surgical practice, e.g., the peeling of a specific area of the membrane on the fundus, the ophthalmic surgeons routinely and purposefully move the RCMs of each instrument, which is called *orbital manipulation*. The human eye has the freedom to rotate around its center, and surgeons take advantage of orbital manipulation to view and approach specific areas in the eye without moving the patient. Despite this widespread use in surgical practice, notably, only the group of [7], [13], and [14] has addressed this topic[1].

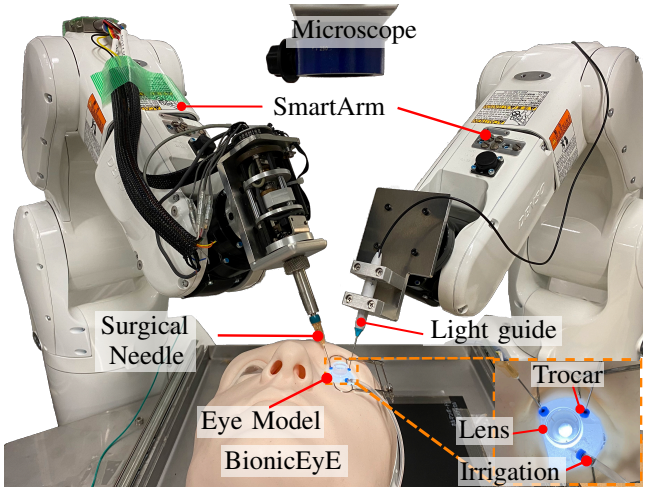

Fig. 1. The vitreoretinal setup of the SmartArm robotic system [12]. The experiments described in Section VI-C were conducted without the face, as it was not made to consider orbital manipulation.

In our group, we have been developing a versatile surgical robotic system for constrained workspaces, called the SmartArm surgical robotic system. The SmartArm system has already been validated using realistic phantoms in some types of surgery [12], [15] and has shown to have enough accuracy for vitreoretinal procedures [16]. The setup of the SmartArm system for vitreoretinal surgery is shown in Fig. 1.

To improve the safety and efficiency of robot-assisted vitreoretinal surgery, we have been working on automation [17]. Our technique also naturally allows for the semi-autonomous scenario where the surgeon tele-operates one of the instruments, and the system autonomously controls the other one, which is a light guide. This semi-autonomous scenario has the potential to improve the efficiency of surgical procedures and possibly lead to new surgical techniques by setting the one hand of the surgeon free.

In this work, we take our semi-autonomous system one step further and add autonomous orbital manipulation. By letting the eye autonomously rotate with respect to the motion of the instruments, surgeons can perform vitreoretinal tasks in a wider workspace without moving the patient.

This research was funded in part by the ImPACT Program of the Council for Science, Technology and Innovation (Cabinet Office, Government of Japan), and in part by the Mori Manufacturing Research and Technology Foundation.

(*Corresponding author:* Murilo M. Marinho)

Yuki Koyama, Murilo M. Marinho, and Kanako Harada are with the Department of Mechanical Engineering, the University of Tokyo, Tokyo, Japan. `Emails:{yuuki-koyama581, murilo, kanakoharada}@g.ecc.u-tokyo.ac.jp`.

[1]To the best of the authors' knowledge, the term *orbital manipulation* was first used in a robotics context in [7].

A. Related works

The automation of vitreoretinal tasks is an active research field. In recent years, He *et al.* [18] performed the bimanual control of instruments and proposed an automatic light pipe actuation system. Kim *et al.* [19] automated a tool-navigation task using deep imitation learning. Shin *et al.* [20] tackled the semi-autonomous extraction of lens fragments. Dehghani *et al.* [21] achieved autonomous docking of the instrument to the trocar.

Regarding object manipulation, some works addressed rigid multibody systems [22], [23] and collaborative deformable tissue manipulation [24]. However, these strategies cannot be directly applied to orbital manipulation, where the instruments penetrate the eyeball instead of grabbing it.

To the best of the authors' knowledge, the works closest to our objectives are the ones from Wei *et al.* [13], where they proposed the mathematical model of orbital manipulation by separating intraocular manipulation from orbital manipulation, and Yu *et al.* [14] from the same group, where they demonstrated their method with a physical model.

In their mathematical model, effective for their purposes, intraocular and orbital manipulation were controlled individually. Our purpose is, instead, to automate orbital manipulation in a transparent way without any change in the description of the task. This autonomous orbital manipulation also requires the definition of hard limits for the motion of the eye, which cannot be achieved by prior work. In this context, we propose a new control strategy for orbital manipulation using inequality constraints based on the vector-field inequalities (VFIs) methodology [25].

B. Statement of contributions

The main contributions of this work are:

1) new VFIs for orbital manipulation based on new distance functions and Jacobians unique to this task, and
2) simulation and experimental results in a physical robotic system to evaluate the effects of orbital manipulation and its feasibility.

II. Problem Statement

Fig. 1 shows the vitreoretinal surgical robotic setup of the SmartArm system. In this work, a surgical needle $(25\,\mathrm{G})$ was used as a dominant surgical instrument. Let the robot that holds the surgical needle be R1, with joint values $\boldsymbol{q}_1 \in \mathbb{R}^{1\times n_1}$, and the robot that holds the light guide be R2, with joint values $\boldsymbol{q}_2 \in \mathbb{R}^{1\times n_2}$. A vitreoretinal surgical phantom with realistic physical properties (BionicEyE [26]) is placed between the two robots. The instruments are inserted into the eye model through ophthalmic trocars. As in surgical practice, a disposable flat lens is placed on the eye model to provide the correct view of the workspace. Images of the workspace are obtained through an ophthalmic microscope placed above the BionicEyE.

We have already considered various requirements unique to robot-assisted vitreoretinal surgery [17]. In this work, our goal is to autonomously perform orbital manipulation to view unseen areas on the fundus without moving the patient.

III. Mathematical background

In this section, we summarize the required background in quaternion algebra, constrained optimization, and VFIs.

A. Quaternions and operators

The quaternion set is

$$\mathbb{H} \triangleq \left\{ h_1 + \hat{\imath} h_2 + \hat{\jmath} h_3 + \hat{k} h_4 \,:\, h_1, h_2, h_3, h_4 \in \mathbb{R} \right\},$$

where $\hat{\imath}^2 = \hat{\jmath}^2 = \hat{k}^2 = \hat{\imath}\hat{\jmath}\hat{k} = -1$. Elements of the set $\mathbb{H}_p \triangleq \{\boldsymbol{h} \in \mathbb{H} : \mathrm{Re}\,(\boldsymbol{h}) = 0\}$ represent translations in $\mathbb{R}^3$. The set of quaternions with unit norm, $\mathbb{S}^3 \triangleq \{\boldsymbol{r} \in \mathbb{H} : \|\boldsymbol{r}\| = 1\}$, represent rotations. We use the operator v_4 to map a quaternion $\boldsymbol{h} \in \mathbb{H}$ into a column vector $\mathbb{R}^4$. Moreover, the Hamilton operators $\overset{+}{\boldsymbol{H}}_4$ and $\overset{-}{\boldsymbol{H}}_4$ [27, Def. 2.1.6] satisfy $\mathrm{v}_4\left(\boldsymbol{h}\boldsymbol{h}'\right) = \overset{+}{\boldsymbol{H}}_4(\boldsymbol{h})\,\mathrm{v}_4\left(\boldsymbol{h}'\right) = \overset{-}{\boldsymbol{H}}_4\left(\boldsymbol{h}'\right)\mathrm{v}_4(\boldsymbol{h})$, $\boldsymbol{C}_4 = \mathrm{diag}(1, -1, -1, -1)$ satisfies $\mathrm{v}_4(\boldsymbol{h}^*) = \boldsymbol{C}_4\,\mathrm{v}_4(\boldsymbol{h})$, and $\overline{\boldsymbol{S}}$ [25, Eq. (3)] has the properties $\mathrm{v}_4\left(\boldsymbol{h}\times\boldsymbol{h}'\right) = \overline{\boldsymbol{S}}(\boldsymbol{h})\,\mathrm{v}_4\left(\boldsymbol{h}'\right) = \overline{\boldsymbol{S}}\left(\boldsymbol{h}'\right)^T\mathrm{v}_4(\boldsymbol{h})$ for $\boldsymbol{h}$, $\boldsymbol{h}' \in \mathbb{H}_p$.

B. Constrained optimization algorithm

We control the translations of the instruments' tips using a centralized kinematic control strategy [15]. Let $\tilde{\boldsymbol{t}}_i \triangleq \tilde{\boldsymbol{t}}_i(\boldsymbol{q}_i) = \boldsymbol{t}_i - \boldsymbol{t}_{i,\mathrm{d}}$ be the translation error between the current translation $\boldsymbol{t}_{\mathrm{i}} \in \mathbb{H}_p$ and the desired translation $\boldsymbol{t}_{i,\mathrm{d}} \in \mathbb{H}_p$ of the i-th robot's end effector, with $i \in \{1, 2\}$. Then, the desired control signal, $\boldsymbol{u} = \begin{bmatrix}\boldsymbol{u}_1^T & \boldsymbol{u}_2^T\end{bmatrix}^T$, is obtained as

$$\begin{aligned}\boldsymbol{u} \in \arg\min_{\dot{\boldsymbol{q}}}\ & \beta\left(f_{\mathrm{t},1} + f_{\lambda,1}\right) + (1-\beta)\left(f_{\mathrm{t},2} + f_{\lambda,2}\right) \\ \text{subject to } & \boldsymbol{W}\dot{\boldsymbol{q}} \preceq \boldsymbol{w},\end{aligned} \tag{1}$$

in which $\boldsymbol{q} = \begin{bmatrix}\boldsymbol{q}_1^T & \boldsymbol{q}_2^T\end{bmatrix}^T$, $f_{\mathrm{t,i}} \triangleq \left\|\boldsymbol{J}_{\boldsymbol{t}_i}\dot{\boldsymbol{q}}_i + \eta\,\mathrm{v}_4\left(\tilde{\boldsymbol{t}}_i\right)\right\|_2^2$ are the cost functions related to the translation errors, $f_{\lambda,i} \triangleq \lambda\|\dot{\boldsymbol{q}}_i\|_2^2$ are the cost functions related to the joint velocity norm, and $\boldsymbol{J}_{\boldsymbol{t}_i} \in \mathbb{R}^{4\times n_i}$ are the translation Jacobians [28] that satisfy $\mathrm{v}_4\left(\dot{\boldsymbol{t}}_i\right) = \boldsymbol{J}_{\boldsymbol{t}_i}\dot{\boldsymbol{q}}_i$. In addition, $\eta \in (0, \infty) \subset \mathbb{R}$ is a tunable gain, $\lambda \in [0, \infty) \subset \mathbb{R}$ is the damping factor, and $\beta \in [0,\,1] \subset \mathbb{R}$ is a weight that defines the priority between the two robots. The r inequality constraints $\boldsymbol{W}\dot{\boldsymbol{q}} \preceq \boldsymbol{w}$, in which $\boldsymbol{W} \triangleq \boldsymbol{W}(\boldsymbol{q}) \in \mathbb{R}^{r\times(n_1+n_2)}$ and $\boldsymbol{w} \triangleq \boldsymbol{w}(\boldsymbol{q}) \in \mathbb{R}^r$, are used to generate active constraints using VFIs [25].

C. Vector-field-inequalities method

The VFI method [25] uses signed distance functions $d \triangleq d(\boldsymbol{q}, t) \in \mathbb{R}$ between two geometric primitives. The time-derivative of the distance is

$$\dot{d} = \underbrace{\frac{\partial\left(d(\boldsymbol{q}, t)\right)}{\partial \boldsymbol{q}}}_{\boldsymbol{J}_d}\dot{\boldsymbol{q}} + \zeta(t),$$

where $\boldsymbol{J}_d \in \mathbb{R}^{1\times(n_1+n_2)}$ is the distance Jacobian and $\zeta(t) = \dot{d} - \boldsymbol{J}_d\dot{\boldsymbol{q}}$ is the residual that contains the distance dynamics unrelated to $\dot{\boldsymbol{q}}$. Then, by using a safe distance $d_{\text{safe}} \triangleq d_{\text{safe}}(t) \in [0, \infty)$, we define an error $\tilde{d} \triangleq \tilde{d}(\boldsymbol{q}, t) = d_{\text{safe}} - d$ to generate safe zones or $\tilde{d} \triangleq d - d_{\text{safe}}$ to generate restricted zones. With these definitions, and given $\eta_d \in [0, \infty)$, the

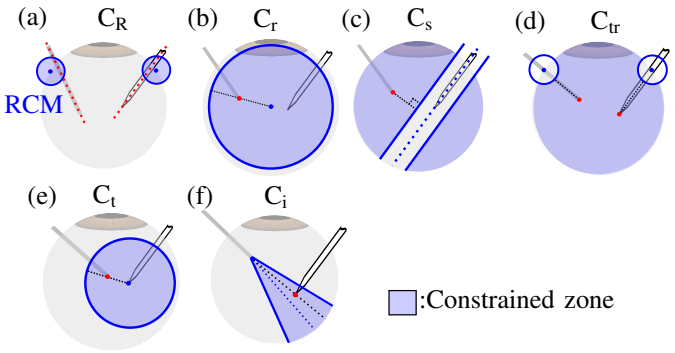

Fig. 2. The illustrations of the geometric primitives used to enforce the constraints for safety and the autonomous control of the light guide.

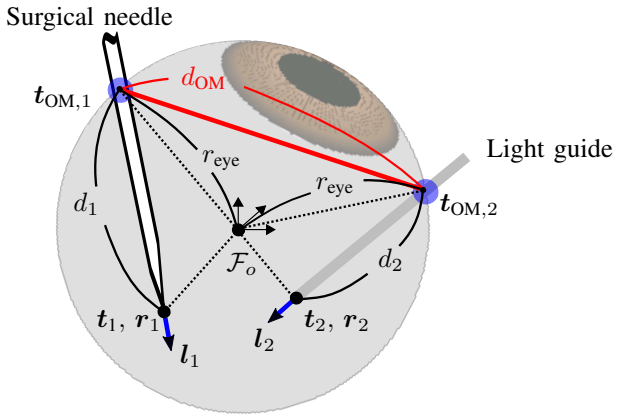

Fig. 3. The geometric relationships for the proposed orbital manipulation.

signed distance dynamics is constrained by $\dot{\tilde{d}} \geq -\eta_d \tilde{d}$ in both cases, which actively constrains the robot motion only in the direction approaching the boundary between the primitives so that the primitives do not collide. That is, the following constraint is used to generate safe zones,

$$\boldsymbol{J}_d \dot{\boldsymbol{q}} \leq \eta_d \tilde{d} - \zeta_{\text{safe}}(t), \tag{2}$$

for $\zeta_{\text{safe}}(t) \triangleq \zeta(t) - \dot{d}_{\text{safe}}$. Alternatively, restricted zones are generated by

$$-\boldsymbol{J}_d \dot{\boldsymbol{q}} \leq \eta_d \tilde{d} + \zeta_{\text{safe}}(t). \tag{3}$$

IV. Robot-Assisted Vitreoretinal Surgery

In our previous work [17], we proposed a control strategy for robot-assisted vitreoretinal surgery without orbital manipulation, including the autonomous coordinated control of the light guide. This section summarizes the relevant parts of [17] used in this work.

Our control strategy relies on the constrained optimization problem described in Section III-B as follows

$$\boldsymbol{u} \in \arg\min_{\dot{\boldsymbol{q}}} \beta(f_{t,1} + f_{\lambda,1}) + (1-\beta)(f_{t,2} + f_{\lambda,2}) \tag{4}$$

$$\text{subject to } \begin{bmatrix} \boldsymbol{W}_{\text{safe}} \\ \boldsymbol{W}_{\text{lg}} \end{bmatrix} \dot{\boldsymbol{q}} \preceq \begin{bmatrix} \boldsymbol{w}_{\text{safe}} \\ \boldsymbol{w}_{\text{lg}} \end{bmatrix}, \tag{5}$$

where $\boldsymbol{t}_{2,\text{d}} = 0$, $\beta = 0.99$, $\eta = 140$, and $\lambda = 0.001$. The desired translation of the surgical needle, $\boldsymbol{t}_{1,\text{d}}$, is determined by the operator or a predefined trajectory. The inequality constraints are used to enforce the constraints to ensure safety, $\boldsymbol{W}_{\text{safe}}\dot{\boldsymbol{q}} \preceq \boldsymbol{w}_{\text{safe}}$, and the constraints for the autonomous control of the light guide, $\boldsymbol{W}_{\text{lg}}\dot{\boldsymbol{q}} \preceq \boldsymbol{w}_{\text{lg}}$.

The inequality constraints $\boldsymbol{W}_{\text{safe}}\dot{\boldsymbol{q}} \preceq \boldsymbol{w}_{\text{safe}}$ enforce the following constraints for safe vitreoretinal tasks

- C_R: the shafts of the instruments must always pass through their respective insertion points.
- C_r: the light guide's tip must never touch the retina.
- C_s: the instruments' shafts must never collide with each other.
- C_{tr}: the instruments' tips must always remain inside the eye.
- C_m: the robots must never collide with the microscope.
- C_{ro}: the robots must never collide with each other.
- C_j: The robots' joint values must never exceed their limits.

Fig. 2-(a), (b), (c), and (d) illustrate the geometrical primitives we use to enforce C_R, C_r, C_s, C_{tr} using VFIs. Details are given in [17, Section VIII].

The inequality constraints $\boldsymbol{W}_{\text{lg}}\dot{\boldsymbol{q}} \preceq \boldsymbol{w}_{\text{lg}}$ enforce the following constraints to autonomously control the light guide

- C_t: the needle's tip must be illuminated sufficiently.
- C_i: the needle's tip must be illuminated at all times.

Fig. 2-(e), (f) illustrate the geometrical primitives that enforce these constraints. Details are given in [17, Section IX].

V. Proposed Orbital Manipulation Strategy

In this section, we describe the main contribution of this work. Orbital manipulation involves systematically moving the RCM positions of both instruments in a coordinated way, such that the eye rotates about its center. Orbital manipulation is frequently used by surgeons, for instance, during the vitrectomy to check if there are no vitreous cortex remnants. Given that the microscope and patient cannot be frequently moved during the surgical procedure, orbital manipulation is the only way to reach certain parts of the fundus and other relevant eye structures.

A. Orbital manipulation VFI

In geometrical terms, orbital manipulation is ensured by keeping the relative position between the RCMs of each instrument while they otherwise freely move. Let the distance between the RCMs be $d_{\text{OM}} \in \mathbb{R}^+$ as shown in Fig. 3, we constrain the squared distance[2] $D_{\text{OM}}(\boldsymbol{q}(t)) \triangleq D_{\text{OM}} = d_{\text{OM}}^2$ as follows

$$-D_{\text{safe}} \leq D_{\text{OM}} - D_{\text{OM,init}} \leq D_{\text{safe}} \iff$$
$$\underbrace{D_{\text{OM}} - (D_{\text{OM,init}} - D_{\text{safe}})}_{\tilde{D}^+_{\text{OM}}} \geq 0, \ \underbrace{(D_{\text{OM,init}} + D_{\text{safe}}) - D_{\text{OM}}}_{\tilde{D}^-_{\text{OM}}} \geq 0, \tag{6}$$

[2]We use the squared distance since its time derivative, which we calculate in Section V-C, is defined everywhere.

where $D_{\text{safe}} = 0.5\,\text{mm}$ and $D_{\text{OM,init}} = D_{\text{OM}}(\boldsymbol{q}(t))|_{t=0}$ are constants. Then, based on (2) and (3), these constraints in terms of joint velocities become

$$\begin{bmatrix} -\boldsymbol{J}_{\text{OM}} \\ \boldsymbol{J}_{\text{OM}} \end{bmatrix} \dot{\boldsymbol{q}} \leq \eta_{\text{OM}} \begin{bmatrix} \tilde{D}_{\text{OM}}^{+} \\ \tilde{D}_{\text{OM}}^{-} \end{bmatrix}, \tag{7}$$

where $\eta_{\text{OM}} = 0.1$, and $\boldsymbol{J}_{\text{OM}} \in \mathbb{R}^{1\times n}$ is the orbital manipulation Jacobian that relates the joint velocities $\dot{\boldsymbol{q}}$ to the time derivative of $\tilde{D}_{\text{OM}}^{+}$ and $\tilde{D}_{\text{OM}}^{-}$ in the form of $\dot{\tilde{D}}_{\text{OM}}^{+} = \boldsymbol{J}_{\text{OM}}\dot{\boldsymbol{q}}$ and $\dot{\tilde{D}}_{\text{OM}}^{-} = -\boldsymbol{J}_{\text{OM}}\dot{\boldsymbol{q}}$, respectively. To enforce (7), we have to find D_{OM} and $\boldsymbol{J}_{\text{OM}}$. We address this in Section V-B and V-C.

B. Orbital manipulation squared distance

The goal of this section is to find the distance function D_{OM} as a function of $\boldsymbol{q}$ to enforce (7). We use the geometric relationships shown in Fig. 3. Let the world reference-frame $\mathcal{F}_o$ be at the center of the eyeball, and let the translations of the RCM points of both instruments be $\boldsymbol{t}_{\text{OM},i}(\boldsymbol{q}_i) \triangleq \boldsymbol{t}_{\text{OM},i} \in \mathbb{H}_p \;\; (i = 1,\, 2)$. Then, we have

$$D_{\text{OM}} = \left\|\boldsymbol{t}_{\text{OM},1} - \boldsymbol{t}_{\text{OM},2}\right\|^2. \tag{8}$$

Next, we assume that, without loss of generality, $\boldsymbol{l}_i(\boldsymbol{q}_i) \triangleq \boldsymbol{l}_i \in \mathbb{S}^3 \cap \mathbb{H}_p$ are the directions of the $z-$axes of the instruments pointing inside the eye and given by

$$\boldsymbol{l}_i = \boldsymbol{r}_i \hat{k}\,(\boldsymbol{r}_i)^*, \tag{9}$$

where $\boldsymbol{r}_i(\boldsymbol{q}_i) \triangleq \boldsymbol{r}_i \in \mathbb{S}^3$ is the rotation of the instrument. Moreover, letting the distances between the tips and the RCM positions be $d_i(\boldsymbol{q}_i) \triangleq d_i \in \mathbb{R}$, we have

$$\boldsymbol{t}_{\text{OM},i} = \boldsymbol{t}_i - d_i\boldsymbol{l}_i. \tag{10}$$

Using the law of cosines, the radius of the eyeball $r_{\text{eye}} \in \mathbb{R}^+ - \{0\}$, and (10), we have

$$\begin{aligned} d_i^2 \;&= \|\boldsymbol{t}_i\|^2 + r_{\text{eye}}^2 - 2\langle \boldsymbol{t}_i, \boldsymbol{t}_{\text{OM},i}\rangle \\ &= r_{\text{eye}}^2 - \|\boldsymbol{t}_i\|^2 + 2d_i\langle \boldsymbol{t}_i, \boldsymbol{l}_i\rangle \\ \iff & d_i^2 - 2\langle \boldsymbol{t}_i, \boldsymbol{l}_i\rangle d_i + \|\boldsymbol{t}_i\|^2 - r_{\text{eye}}^2 = 0 \\ \iff & d_i = \langle \boldsymbol{t}_i, \boldsymbol{l}_i\rangle \pm \sqrt{\langle \boldsymbol{t}_i, \boldsymbol{l}_i\rangle^2 - \|\boldsymbol{t}_i\|^2 + r_{\text{eye}}^2}. \end{aligned}$$

Because of our definition of the direction for $\boldsymbol{l}_i$, only the positive value is relevant.[3] Therefore, we have

$$d_i = \langle \boldsymbol{t}_i, \boldsymbol{l}_i\rangle + \underbrace{\sqrt{\langle \boldsymbol{t}_i, \boldsymbol{l}_i\rangle^2 - \|\boldsymbol{t}_i\|^2 + r_{\text{eye}}^2}}_{h_1}. \tag{11}$$

C. Orbital manipulation Jacobian

Our next goal is to find the corresponding Jacobian $\boldsymbol{J}_{\text{OM}}$ to enforce (7). Since the time derivatives of $\tilde{D}_{\text{OM}}^{+}$ and $\tilde{D}_{\text{OM}}^{-}$ are $\dot{D}_{\text{OM}}$ and $-\dot{D}_{\text{OM}}$, we can get $\boldsymbol{J}_{\text{OM}}$ by finding the time derivative of D_{OM} with respect to the joint velocities $\dot{\boldsymbol{q}}$. From (8), we have

$$\dot{D}_{\text{OM}} = 2\,\text{v}_4\left(\boldsymbol{t}_{\text{OM},1} - \boldsymbol{t}_{\text{OM},2}\right)^T \text{v}_4\left(\dot{\boldsymbol{t}}_{\text{OM},1} - \dot{\boldsymbol{t}}_{\text{OM},2}\right). \tag{12}$$

From (10), the time derivative of $\boldsymbol{t}_{\text{OM},i} \;\; (i = 1,\, 2)$ is

$$\text{v}_4\left(\dot{\boldsymbol{t}}_{\text{OM},i}\right) = \boldsymbol{J}_{\boldsymbol{t}_i}\dot{\boldsymbol{q}}_i - \text{v}_4\left(\dot{d}_i\boldsymbol{l}_i + d_i\dot{\boldsymbol{l}}_i\right). \tag{13}$$

Then, we have to find $\dot{\boldsymbol{l}}_i$ and $\dot{d}_i$. From (9), we get

$$\text{v}_4\left(\dot{\boldsymbol{l}}_i\right) = \underbrace{\left(\bar{\boldsymbol{H}}_4\left(\hat{k}\,(\boldsymbol{r}_i)^*\right) + \overset{+}{\boldsymbol{H}}_4\left(\boldsymbol{r}_i\hat{k}\right)\boldsymbol{C}_4\right)\boldsymbol{J}_{\boldsymbol{r}_i}}_{\boldsymbol{J}_{\boldsymbol{l}_i}}\dot{\boldsymbol{q}}_i, \tag{14}$$

where $\boldsymbol{J}_{\boldsymbol{r}_i} \in \mathbb{R}^{1\times n_i}$ is the rotation Jacobian [28] that satisfies $\dot{\boldsymbol{r}}_i = \boldsymbol{J}_{\boldsymbol{r}_i}\dot{\boldsymbol{q}}_i$. As for $\dot{d}_i$, from (11), we have

$$\dot{d}_i = \overbrace{\left\langle \dot{\boldsymbol{t}}_i, \boldsymbol{l}_i\right\rangle + \left\langle \boldsymbol{t}_i, \dot{\boldsymbol{l}}_i\right\rangle}^{h_2} + \dot{h}_1. \tag{15}$$

Then, considering h_1 is a positive value,[4] we get

$$\begin{aligned} \dot{h}_1 &= \frac{2\left(\left\langle \dot{\boldsymbol{t}}_i, \boldsymbol{l}_i\right\rangle + \left\langle \boldsymbol{t}_i, \dot{\boldsymbol{l}}_i\right\rangle\right) - 2\left\langle \boldsymbol{t}_i, \dot{\boldsymbol{t}}_i\right\rangle}{h_1} \\ &= \frac{1}{h_1}\left(2h_2 - 2\,\text{v}_4\left(\boldsymbol{t}_i\right)^T \text{v}_4\left(\dot{\boldsymbol{t}}_i\right)\right), \end{aligned}$$

and, from (14),

$$h_2 = \underbrace{\left(\text{v}_4\left(\boldsymbol{l}_i\right)^T\boldsymbol{J}_{\boldsymbol{t}_i} + \text{v}_4\left(\boldsymbol{t}_i\right)^T\boldsymbol{J}_{\boldsymbol{l}_i}\right)}_{\boldsymbol{J}_{h_2}}\dot{\boldsymbol{q}}_i. \tag{16}$$

Therefore, we have

$$\dot{h}_1 = \underbrace{\left(2\boldsymbol{J}_{h_2} - 2\,\text{v}_4\left(\boldsymbol{t}_i\right)^T\boldsymbol{J}_{\boldsymbol{t}_i}\right)}_{\boldsymbol{J}_{h_1}}\dot{\boldsymbol{q}}_i. \tag{17}$$

We can now work backwards to find the corresponding Jacobian $\boldsymbol{J}_{\text{OM}}$. By substituting (16) and (17) into (15), we have

$$\dot{d}_i = \underbrace{\left(\boldsymbol{J}_{h_2} + \boldsymbol{J}_{h_1}\right)}_{\boldsymbol{J}_{d_i}}\dot{\boldsymbol{q}}_i. \tag{18}$$

Moreover, substituting (14) and (18) into (13) results in

$$\text{v}_4\left(\dot{\boldsymbol{t}}_{\text{OM},i}\right) = \underbrace{\left(\boldsymbol{J}_{\boldsymbol{t}_i} - \text{v}_4\left(\boldsymbol{l}_i\right)\boldsymbol{J}_{d_i} + d_i\boldsymbol{J}_{\boldsymbol{l}_i}\right)}_{\boldsymbol{J}_{\boldsymbol{t}_{\text{OM},i}}}\dot{\boldsymbol{q}}_i. \tag{19}$$

Finally, from (12) and (19), we find

$$\dot{D}_{\text{R}} = \underbrace{2\,\text{v}_4\left(\boldsymbol{t}_{\text{OM},1} - \boldsymbol{t}_{\text{OM},2}\right)^T\begin{bmatrix} \boldsymbol{J}_{\boldsymbol{t}_{\text{OM},1}} & -\boldsymbol{J}_{\boldsymbol{t}_{\text{OM},2}} \end{bmatrix}}_{\boldsymbol{J}_{\text{OM}}}\dot{\boldsymbol{q}}. \tag{20}$$

D. Constraints for safe orbital manipulation

When the eye is autonomously rotated, safe limits must be enforced to preserve the integrity of the eye muscles. To do so, we also propose additional constraints.

Fig. 4 shows the constraints C_{rot1} and C_{rot2}. These constraints prevent the eyeball from rotating beyond a certain angle. To this purpose, we constrain the RCM positions $\boldsymbol{t}_{\text{OM},1}$ and $\boldsymbol{t}_{\text{OM},2}$ to be within a certain distance from the planes

[3] The other value has an interesting mathematical meaning, because it will be the other point in the sphere that satisfies this same equation for $-\boldsymbol{l}_i$.

[4] Since the tip of the instrument is kept inside the eyeball, $r_{\text{eye}}^2 > \|\boldsymbol{t}_i\|^2 \iff r_{\text{eye}}^2 - \|\boldsymbol{t}_i\|^2 > 0$.

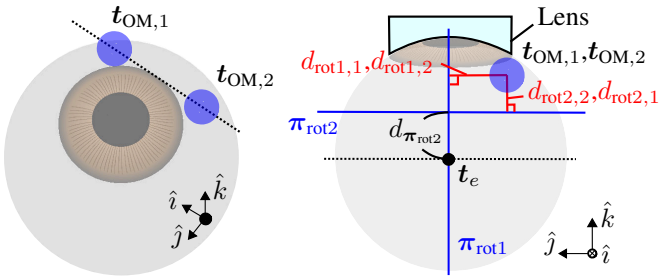

Fig. 4. Geometrical primitives used to enforce the constraints to limit the rotation of the eyeball, C_{rot1} and C_{rot2}.

$\boldsymbol{\pi}_{\text{rot1}}$ and $\boldsymbol{\pi}_{\text{rot2}}$. The plane $\boldsymbol{\pi}_{\text{rot1}}$ is the plane perpendicular to the $x-$axis and contains the center of the eyeball. The plane $\boldsymbol{\pi}_{\text{rot2}}$ is the plane perpendicular to the $z-$axis and $d_{\boldsymbol{\pi}_{\text{rot2}}}$ away from the $xy-$plane. The distance $d_{\boldsymbol{\pi}_{\text{rot2}}}$ is half the radius of the eyeball.

These constraints can be enforced using the signed distances and Jacobians proposed in [25, Eq. (57), (59)]. Let the signed distances and Jacobians between $\boldsymbol{t}_{\text{OM},1}$ and $\boldsymbol{\pi}_{\text{rot1}}$, $\boldsymbol{\pi}_{\text{rot2}}$ be $d_{\text{rot1},1}, d_{\text{rot2},1} \in \mathbb{R}$ and $\boldsymbol{J}_{\text{rot1},1}, \boldsymbol{J}_{\text{rot2},1} \in \mathbb{R}^{1\times n_1}$, and the signed distances and Jacobians between $\boldsymbol{t}_{\text{OM},2}$ and $\boldsymbol{\pi}_{\text{rot1}}$, $\boldsymbol{\pi}_{\text{rot2}}$ be $d_{\text{rot1},2}, d_{\text{rot2},2} \in \mathbb{R}$ and $\boldsymbol{J}_{\text{rot1},2}, \boldsymbol{J}_{\text{rot2},2} \in \mathbb{R}^{1\times n_2}$. Then, to enforce $C_{\text{rot}j}$ $(j = 1, 2)$, we can use

$$\begin{bmatrix} -\boldsymbol{J}_{\text{rot}j,1} & \boldsymbol{O}_{1\times n_1} \\ \boldsymbol{O}_{1\times n_2} & -\boldsymbol{J}_{\text{rot}j,2} \end{bmatrix} \dot{\boldsymbol{q}} \leq \eta_{\text{rot}} \begin{bmatrix} d_{\text{rot}j,1} \\ d_{\text{rot}j,2} \end{bmatrix}, \tag{21}$$

where $\eta_{\text{rot}} = 1.0$.

VI. Experiments

We designed one simulation study and one experiment to evaluate our proposed control strategy. First, we describe the simulation results to evaluate the influence of the orbital manipulation on the manipulability of our system. Then, we show experimental results to demonstrate the feasibility of our method and the improvement in the microscopic field of view enabled by the orbital manipulation when using the physical robotic system.

A. Setup

The physical robotic setup shown in Fig. 1 was used for the experiment. To observe the orbital manipulation, the experiment was conducted without the face of the BionicEyE. For the simulation study, this setup was replicated in CoppeliaSim (Coppelia Robotics, Switzerland). Communication with the robot was enabled by the SmartArmStack[5]. The quaternion algebra and robot kinematics were implemented using DQ Robotics [29] for Python3. The calibration of the system and the registration of the initial RCM positions were performed as described in [17, Section X].

B. Simulation: Evaluation of manipulability

Inequality constraints, in general, can increase or reduce the manipulability of the system in complex ways, and currently, there is no systematic way of analyzing manipulability

[5]https://github.com/SmartArmStack

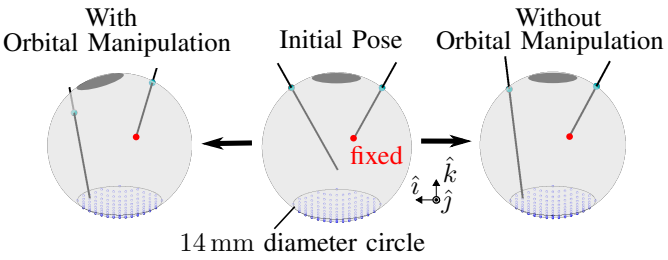

Fig. 5. Positioning with and without the proposed orbital manipulation in the simulation study.

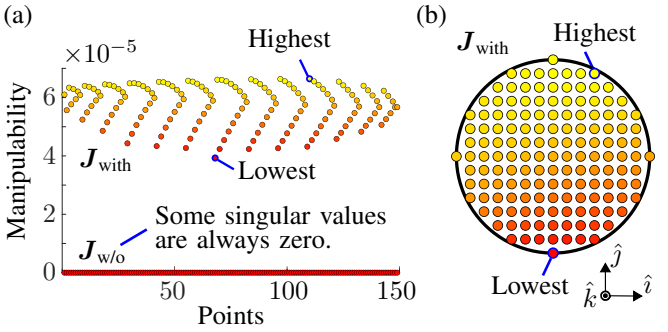

Fig. 6. Manipulability measures [30] of $\boldsymbol{J}_{\text{with}}$ and $\boldsymbol{J}_{\text{w/o}}$ calculated at 149 points that cover a 14 mm diameter area around the fundus in simulation.

in this case. In this study, to assess the impact of the proposed orbital manipulation on the manipulability of the system, the manipulability measure proposed in [30] was used as a strict lower-bound to compare our proposed orbital manipulation strategy and conventional fixed RCM-based control.

As shown in Fig. 5, the procedure was as follows. First, the surgical needle's tip was positioned to a point on the fundus with and without enforcing the orbital manipulation. Then, the manipulability measures after positioning were calculated and compared. Positioning was conducted from the same initial pose to 149 positions covering a 14 mm diameter circle, which is the double size of the usual target area. To make conditions equal, the tip of the light guide was commanded to be still.

For a Jacobian $\boldsymbol{J}$, the manipulability measure is calculated as

$$\omega = \sqrt{\det\left|\boldsymbol{J}\boldsymbol{J}^T\right|}, \tag{22}$$

which is related to the manipulability ellipsoid proposed in [30]. Compatible with the original definition, we used the following augmented Jacobians

$$\boldsymbol{J}_{\text{w/o}} = \begin{bmatrix} \boldsymbol{J}_{\boldsymbol{t}_1} & \boldsymbol{O}_{3\times n_2} \\ \boldsymbol{O}_{3\times n_1} & \boldsymbol{J}_{\boldsymbol{t}_2} \\ \boldsymbol{J}_{\boldsymbol{t}_{\text{OM},1}} & \boldsymbol{O}_{1\times n_2} \\ \boldsymbol{O}_{1\times n_1} & \boldsymbol{J}_{\boldsymbol{t}_{\text{OM},2}} \end{bmatrix} \text{ and } \boldsymbol{J}_{\text{with}} = \begin{bmatrix} \boldsymbol{J}_{\boldsymbol{t}_1} & \boldsymbol{O}_{3\times n_2} \\ \boldsymbol{O}_{3\times n_1} & \boldsymbol{J}_{\boldsymbol{t}_2} \\ & \boldsymbol{J}'_{\text{OM}} \end{bmatrix},$$

for the fixed-RCM evaluation and the orbital manipulation evaluation, respectively. Note that $\boldsymbol{J}_{\boldsymbol{t}_i}$ are the translation Jacobians, and $\boldsymbol{J}_{\boldsymbol{t}_{\text{OM},i}}$ are as found in (19). Moreover, $\boldsymbol{J}'_{\text{OM}}$ is the proposed orbital manipulation Jacobian that satisfies $\boldsymbol{J}'_{\text{OM}}\dot{\boldsymbol{q}} = \frac{d}{dt}\left(\|\boldsymbol{t}_{\text{OM},1} - \boldsymbol{t}_{\text{OM},2}\|\right)$. That is because it is well known that, to calculate the manipulability, we need to unify

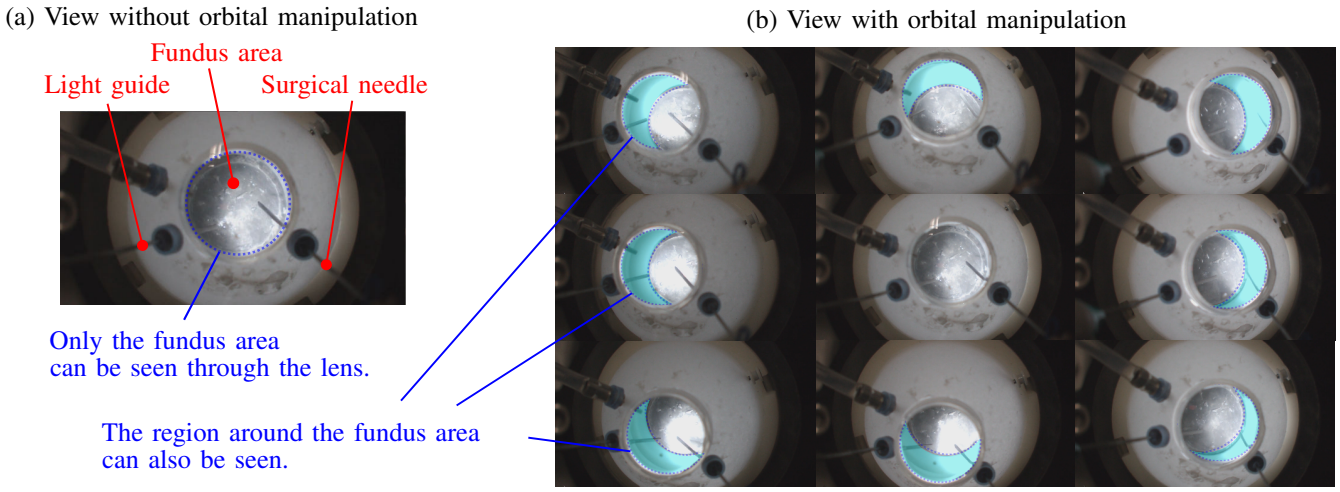

Fig. 7. Comparison between conventional RCM-based control and the proposed orbital manipulation strategy. (a) shows the microscopic view with conventional RCM-based control. The eyeball does not rotate, and the operator could see only the same regions of the fundus of the eye model of the BionicEyE regardless of the motion of the instruments. (b) shows the microscopic view with the proposed autonomous orbital manipulation. Our strategy autonomously rotates the eye model with respect to the motion of the instruments, and the operator could observe the area around the fundus otherwise unseen. The newly visible region was colored in light blue for easier visualization.

the units of the augmented Jacobian. Hence, by letting $h_3 = \|t_{\mathrm{OM},1} - t_{\mathrm{OM},2}\| > 0$, the Jacobian J'_{OM} can be calculated as follows.

$$\dot{h}_3 = \underbrace{\frac{1}{h_3} \mathrm{v}_4 \left(t_{\mathrm{OM},1} - t_{\mathrm{OM},2}\right)^T \begin{bmatrix} J_{t_{\mathrm{OM},1}} & -J_{t_{\mathrm{OM},2}} \end{bmatrix}}_{J'_{\mathrm{OM}}} \dot{q}.$$

1) Results and discussion: Fig. 6-(a) shows the manipulability measures of J_{with} and $J_{\mathrm{w/o}}$ calculated at the 149 points. The figure shows that the orbital manipulation provided higher values of the manipulability measure. The manipulability measure of $J_{\mathrm{w/o}}$ was always zero because one of the singular values related to the fixed RCM constraint was always zero.

Fig. 6-(b) shows the manipulability measures of J_{with} at each point. The manipulability measures of the points away from the RCMs were higher than those of the points near the RCMs. This means that the tip of the surgical needle can smoothly access the points far from the RCMs by moving the RCMs.

C. Experiment: Evaluation of real-world feasibility

This experiment was conducted to show the feasibility of the proposed method and compare it with a conventional approach. In this experiment, the tip of the surgical needle was tele-operatively controlled using an input device (Touch, 3D Systems, USA). The operator arbitrarily moved the tip parallel to the image plane of the microscope in two modes, with the conventional fixed-RCM and the proposed orbital manipulation strategy. The field-of-view of the microscope was larger than in actual surgery for a proper workspace analysis.

1) Results and discussion: As shown in Fig. 7-(a), with the conventional approach, the operator could see only the same region of the fundus of the eye model. On the other hand, as shown in Fig. 7-(b), the orbital manipulation enabled the operator to observe a larger area around the fundus. We also confirmed that the proposed constraints were satisfied, and the orbital manipulation was enforced autonomously with respect to the motion of the tip of the surgical needle.

Moreover, the light guide autonomously followed the tip of the surgical needle during the experiments, and the constraints for safety and the automation of the light guide were also satisfied.

Lastly, it cannot be understated that the proposed orbital manipulation based on VFIs comes at very little cost. In fact, the quadratic programming solver has one less constraint to solve with respect to having two fixed RCMs. In addition, there was no change in task description nor increase in the number of control parameters. Enacting limits on the orbital manipulation increases the number of design parameters, but those are intrinsic to the eye and require no specific tuning.

VII. Conclusion

In this paper, we proposed a new control strategy for orbital manipulation. To achieve this, we derived a new distance function and its corresponding Jacobian to keep the relative position between the RCMs using VFIs. In a simulation and an experiment, we showed that orbital manipulation increased the manipulability of the system and enabled the operator to observe a larger area around the fundus.

Future works include the investigation of the sclera force during orbital manipulation, the consideration of the eyeball pose, and the evaluation of the feasibility of vitreoretinal tasks otherwise impossible without orbital manipulation.

References

[1] S. Singh and C. Riviere, "Physiological tremor amplitude during retinal microsurgery," in *Proceedings of the IEEE 28th Annual Northeast Bioengineering Conference*. IEEE, pp. 171–172. [Online]. Available: https://ieeexplore.ieee.org/document/999520/

[2] I. i. Iordachita, M. D. de Smet, G. Naus, M. Mitsuishi, and C. N. Riviere, "Robotic Assistance for Intraocular Microsurgery: Challenges and Perspectives," *Proceedings of the IEEE*, pp. 1–16. [Online]. Available: https://ieeexplore.ieee.org/document/9771085/

[3] R. A. MacLachlan, B. C. Becker, J. C. Tabares, G. W. Podnar, L. A. Lobes, and C. N. Riviere, "Micron: An Actively Stabilized Handheld Tool for Microsurgery," *IEEE Transactions on Robotics*, vol. 28, no. 1, pp. 195–212. [Online]. Available: https://ieeexplore.ieee.org/document/6084852/

[4] E. Kim, I. Choi, and S. Yang, "Design and Control of Fully Handheld Microsurgical Robot for Active Tremor Cancellation," in *2021 International Conference on Robotics and Automation (ICRA)*, p. 7.

[5] A. Uneri, M. A. Balicki, J. Handa, P. Gehlbach, R. H. Taylor, and I. Iordachita, "New steady-hand Eye Robot with micro-force sensing for vitreoretinal surgery," in *2010 3rd IEEE RAS & EMBS International Conference on Biomedical Robotics and Biomechatronics*. IEEE, pp. 814–819. [Online]. Available: http://ieeexplore.ieee.org/document/5625991/

[6] A. Gijbels, K. Willekens, L. Esteveny, P. Stalmans, D. Reynaerts, and E. Vander Poorten, "Towards a clinically applicable robotic assistance system for retinal vein cannulation," in *2016 6th IEEE International Conference on Biomedical Robotics and Biomechatronics (BioRob)*, pp. 284–291.

[7] W. Wei, R. Goldman, N. Simaan, H. Fine, and S. Chang, "Design and Theoretical Evaluation of Micro-Surgical Manipulators for Orbital Manipulation and Intraocular Dexterity," in *Proceedings 2007 IEEE International Conference on Robotics and Automation*, pp. 3389–3395.

[8] M. A. Nasseri, M. Eder, S. Nair, E. C. Dean, M. Maier, D. Zapp, C. P. Lohmann, and A. Knoll, "The introduction of a new robot for assistance in ophthalmic surgery," in *2013 35th Annual International Conference of the IEEE Engineering in Medicine and Biology Society (EMBC)*, pp. 5682–5685.

[9] J. T. Wilson, M. J. Gerber, S. W. Prince, C.-W. Chen, S. D. Schwartz, J.-P. Hubschman, and T.-C. Tsao, "Intraocular robotic interventional surgical system (IRISS): Mechanical design, evaluation, and master-slave manipulation: Intraocular robotic interventional surgical system (IRISS)," *The International Journal of Medical Robotics and Computer Assisted Surgery*, vol. 14, no. 1, p. e1842. [Online]. Available: http://doi.wiley.com/10.1002/rcs.1842

[10] T. L. Edwards, K. Xue, H. C. M. Meenink, M. J. Beelen, G. J. L. Naus, M. P. Simunovic, M. Latasiewicz, A. D. Farmery, M. D. de Smet, and R. E. MacLaren, "First-in-human study of the safety and viability of intraocular robotic surgery," *Nature Biomedical Engineering*, vol. 2, no. 9, pp. 649–656. [Online]. Available: https://www.nature.com/articles/s41551-018-0248-4

[11] A. Gijbels, J. Smits, L. Schoevaerdts, K. Willekens, E. B. Vander Poorten, P. Stalmans, and D. Reynaerts, "In-Human Robot-Assisted Retinal Vein Cannulation, A World First," *Annals of Biomedical Engineering*, vol. 46, no. 10, pp. 1676–1685. [Online]. Available: http://link.springer.com/10.1007/s10439-018-2053-3

[12] M. M. Marinho, K. Harada, A. Morita, and M. Mitsuishi, "SmartArm: Integration and validation of a versatile surgical robotic system for constrained workspaces," *The International Journal of Medical Robotics and Computer Assisted Surgery*, vol. 16, no. 2, apr 2020. [Online]. Available: https://onlinelibrary.wiley.com/doi/abs/10.1002/rcs.2053

[13] Wei Wei, R. Goldman, H. Fine, Stanley Chang, and N. Simaan, "Performance Evaluation for Multi-arm Manipulation of Hollow Suspended Organs," *IEEE Transactions on Robotics*, vol. 25, no. 1, pp. 147–157. [Online]. Available: http://ieeexplore.ieee.org/document/4694099/

[14] H. Yu, J.-H. Shen, K. M. Joos, and N. Simaan, "Design, calibration and preliminary testing of a robotic telemanipulator for OCT guided retinal surgery," in *2013 IEEE International Conference on Robotics and Automation*. IEEE, pp. 225–231. [Online]. Available: http://ieeexplore.ieee.org/document/6630580/

[15] M. M. Marinho, B. V. Adorno, K. Harada, K. Deie, A. Deguet, P. Kazanzides, R. H. Taylor, and M. Mitsuishi, "A Unified Framework for the Teleoperation of Surgical Robots in Constrained Workspaces," in *2019 International Conference on Robotics and Automation (ICRA)*. IEEE, pp. 2721–2727. [Online]. Available: https://ieeexplore.ieee.org/document/8794363/

[16] Y. Tomiki, M. M. Marinho, Y. Kurose, K. Harada, and M. Mitsuishi, "On the use of general-purpose serial-link manipulators in eye surgery," in *2017 14th International Conference on Ubiquitous Robots and Ambient Intelligence (URAI)*, pp. 540–541.

[17] Y. Koyama, M. M. Marinho, M. Mitsuishi, and K. Harada, "Autonomous Coordinated Control of the Light Guide for Positioning in Vitreoretinal Surgery," *IEEE Transactions on Medical Robotics and Bionics*, vol. 4, no. 1, pp. 156–171, feb 2022.

[18] C. He, E. Yang, N. Patel, A. Ebrahimi, M. Shahbazi, P. Gehlbach, and I. Iordachita, "Automatic Light Pipe Actuating System for Bimanual Robot-Assisted Retinal Surgery," *IEEE/ASME Transactions on Mechatronics*, vol. 25, no. 6, pp. 2846–2857. [Online]. Available: https://ieeexplore.ieee.org/document/9099104/

[19] J. W. Kim, P. Zhang, P. Gehlbach, I. Iordachita, and M. Kobilarov, "Towards Autonomous Eye Surgery by Combining Deep Imitation Learning with Optimal Control," *Proceedings of machine learning research*, vol. 155, pp. 2347–2358. [Online]. Available: https://www.ncbi.nlm.nih.gov/pmc/articles/PMC8549631/

[20] C. Shin, M. J. Gerber, Y.-H. Lee, M. Rodriguez, S. A. Pedram, J.-P. Hubschman, T.-C. Tsao, and J. Rosen, "Semi-Automated Extraction of Lens Fragments Via a Surgical Robot Using Semantic Segmentation of OCT Images With Deep Learning - Experimental Results in Ex Vivo Animal Model," *IEEE Robotics and Automation Letters*, vol. 6, no. 3, pp. 5261–5268.

[21] S. Dehghani, M. Sommersperger, J. Yang, M. Salehi, B. Busam, K. Huang, P. Gehlbach, I. I. Iordachita, N. Navab, and M. A. Nasseri, "ColibriDoc: An Eye-In-Hand Autonomous Trocar Docking System," in *2021 International Conference on Robotics and Automation (ICRA)*, p. 7.

[22] S. Lee, "Dual redundant arm configuration optimization with task-oriented dual arm manipulability," *IEEE Transactions on Robotics and Automation*, vol. 5, no. 1, pp. 78–97.

[23] J.-Y. Wen and L. Wilfinger, "Kinematic manipulability of general constrained rigid multibody systems," *IEEE Transactions on Robotics and Automation*, vol. 15, no. 3, pp. 558–567.

[24] F. Alambeigi, Z. Wang, Y.-h. Liu, R. H. Taylor, and M. Armand, "Toward Semi-autonomous Cryoablation of Kidney Tumors via Model-Independent Deformable Tissue Manipulation Technique," *Annals of Biomedical Engineering*, vol. 46, no. 10, pp. 1650–1662. [Online]. Available: http://link.springer.com/10.1007/s10439-018-2074-y

[25] M. M. Marinho, B. V. Adorno, K. Harada, and M. Mitsuishi, "Dynamic Active Constraints for Surgical Robots Using Vector-Field Inequalities," *IEEE Transactions on Robotics*, vol. 35, no. 5, pp. 1166–1185, oct 2019. [Online]. Available: https://ieeexplore.ieee.org/document/8742769/

[26] S. Omata, Y. Someya, S. Adachi, T. Masuda, T. Hayakawa, K. Harada, M. Mitsuishi, K. Totsuka, F. Araki, M. Takao, M. Aihara, and F. Arai, "A surgical simulator for peeling the inner limiting membrane during wet conditions," *PLOS ONE*, vol. 13, no. 5, p. e0196131. [Online]. Available: https://dx.plos.org/10.1371/journal.pone.0196131

[27] B. V. Adorno, *Robot Kinematic Modeling and Control Based on Dual Quaternion Algebra - Part I: Fundamentals.*

[28] B. V. Adorno, P. Fraisse, and S. Druon, "Dual position control strategies using the cooperative dual task-space framework," in *2010 IEEE/RSJ International Conference on Intelligent Robots and Systems*, pp. 3955–3960.

[29] B. V. Adorno and M. Marques Marinho, "DQ Robotics: A Library for Robot Modeling and Control," *IEEE Robotics and Automation Magazine*, vol. 28, no. 3, pp. 102–116, sep 2021. [Online]. Available: https://ieeexplore.ieee.org/document/9136790/

[30] T. Yoshikawa, "Manipulability of Robotic Mechanisms," *The International Journal of Robotics Research*, vol. 4, no. 2, pp. 3–9. [Online]. Available: https://doi.org/10.1177/027836498500400201